Journal of Power Sources 196 (2011) 3513–3522

Contents lists available at ScienceDirect

Journal of Power Sources

journal homepage: www.elsevier.com/locate/jpowsour

Electrochemical characterization of the surface and methanol electrooxidation on Pt–Rh–Pd ternary alloys

M. Soszko, M. Łukaszewski, Z. Mianowska, A. Czerwiński*

Industrial Chemistry Research Institute, Rydygiera 8, 01-793 Warsaw, Poland

ARTICLE INFO

Article history:
Received 9 November 2010
Received in revised form 9 December 2010
Accepted 11 December 2010
Available online 21 December 2010

Keywords:
Methanol electrooxidation
Palladium alloys
Electron per site
Surface composition
Real surface area

ABSTRACT

Methanol adsorption and electrooxidation have been studied on Pt–Rh–Pd alloys using cyclic voltammetry and chronoamperometry. Pt–Rh–Pd electrodes were prepared by a potentiostatic electrodeposition on a gold wire from chloride solutions. Alloy bulk composition was determined by SEM/EDAX measurements. Alloy surface composition was estimated adapting Rand and Woods's method for homogenous binary noble metal alloys utilizing the potential of surface oxide reduction peak. Electrode real surface area was calculated from the charge due to surface oxide formation/reduction. Methanol was oxidized both in stripping voltammetric experiments and continuously under potentiostatic conditions from 1 M CH_3OH/0.5 M H_2SO_4 solution. The values of electron per site, surface coverage and oxidation potential were used for the characterization of methanol adsorption products. The comparison of these results with analogous data for CO_2 and CO adsorption has revealed high similarity between CO_2 and methanol adsorption products, both consisting of mainly linearly and bridge-bonded CO species, however, with a higher contribution from bridge-bonded CO in the case of methanol. Current densities obtained during continuous methanol oxidation were the highest for Pt–Rh–Pd alloys with initial bulk composition 30.6% Pt, 23.7% Rh, 45.7% Pd, being of the same order as for pure Pt electrode.

1. Introduction

The conception of the fuel cells has been known for nearly two hundred years. First articles illustrating the operation of a device which converts chemical energy directly into electrical current were published at the end of the 1830s [1], and the interest in that field has been growing again since the 1950s. Among various types of low-temperature fuel cells, direct methanol fuel cell (DMFC) with platinum-based anodes has been considered as the most promising energy source for portable electrical devices [2,3]. Simple thermodynamic calculations for the methanol electrooxidation lead to the values of energy density of the order of 6 kWh kg^{-1}, i.e., comparable to those for hydrocarbons or gasoline, and the reversible energy theoretical efficiency of 96.7%, which is far greater than for classical fossil fuels [4]. However, poor kinetics of methanol electrooxidation on platinum is still one of the major problems. Second problematic factor is the oxygen reduction reaction (ORR), which can occur at high overpotentials according to the two-pathway mechanism, depending on the cathode material [2,3,5].

In general, the electrooxidation of methanol can be described as a two-step process, which includes [a] adsorption and dehydrogenation of the alcohol molecule on the electrode surface; [b] oxidation of the adsorbate with the formation of gaseous CO_2 [6,7]. Adsorption of methanol leads to the creation of carbonaceous species, conventionally denoted as CO_{ads}. It is well known that methanol, CO and CO_2 adsorption at single crystal platinum is highly sensitive to its Miller index [7]. Vidal et al. using visible–infrared sum frequency generation vibrational spectroscopy (SFG) have confirmed significant differences between CO/Pt(1 0 0), CO/Pt(1 1 0) and CO/Pt(1 1 1) interfaces in case of gaseous CO adsorption on Pt single crystal electrodes [8]. Except linear and bridge bonded CO molecules, which are the main products of methanol, gaseous CO_2 and CO adsorption, several different structures were also detected on platinum and other noble metals [7,9], namely more reduced species, i.e., COH_{ads} or HCO_{ads} as well as more oxidized ones, i.e., $COOH_{ads}$.

There are many techniques useful in studying the adsorption products on solid electrodes. In addition to classical electrochemical methods, such as cyclic voltammetry (CV) or chronoamperometry (CA), the impedance spectroscopy (IS) [10–12] and electrochemical quartz crystal microbalance (EQCM) [13–15] were applied. The most popular of nonelectrochemical or combined techniques are IR spectroscopy and its varieties (SERS, FTIR) as well as mass spectrometry (MS, DEMS) [16–21]. The results of

* Corresponding author. Tel.: +48 22 568 24 43; fax: +48 22 568 23 90.
E-mail addresses: andrzej.czerwinski@ichp.pl, aczerw@chem.uw.edu.pl (A. Czerwiński).

0378-7753/$ – see front matter © 2011 Elsevier B.V. All rights reserved.
doi:10.1016/j.jpowsour.2010.12.046

the investigations on the kinetics of adsorption and desorption of methanol-derived CO at Pt and Pt–Ru nanoparticles were also obtained by Waszczuk et al. using the radioactive labeling with ^{14}C-methanol [22]. However, radiometric methods are not commonly used because of their great sensitivity to geometric disturbances of the measurement system.

Irreversible adsorption of methanol occurs in the range of 0.05–0.50 V vs SHE, thus adsorbed CO_{ads} species are responsible for "poisoning" of the electrode. The removal of CO_{ads} from the electrode surface requires the presence of atomic oxygen derived from dissociation of water (low pH) or OH^- ions (high pH). In general, a complete methanol electrooxidation at platinum electrodes occurs according to the following equations:

$$Pt + CH_3OH \rightarrow Pt{=}CO(Pt_2 > CO) + 4H^+ + 4e^- \quad (1)$$

$$Pt + H_2O \rightarrow Pt\text{–}OH + H^+ + e^- \quad (2)$$

$$Pt{=}CO + Pt\text{–}OH \rightarrow 2Pt + CO_2 + H^+ + e^- \quad (3)$$

Summary:

$$CH_3OH + H_2O \rightarrow CO_2 + 6H^+ + 6e^- \quad (4)$$

Surface oxides on Pt electrode begin to be formed at potential of 0.7 V vs SHE (Eq. (2)), which is too high for an efficient performance of the cell. In a classical approach Pt–OH species are considered as the oxidant for adsorbed CO. However, Jerkiewicz et al. using the EQCM technique have shown that oxygen adsorption on platinum electrode leads to the creation of $(Pt\text{–}Pt)^{\delta+}\text{–}O_{chem}{}^{\delta-}$ species rather than Pt–OH [23].

One of the most popular ways to improve the kinetics of methanol electrooxidation is the use of platinum alloys with some transition metals. There are many reports on a high electrocatalytic activity of binary and ternary alloys containing Sn, Mo, Ru, Os, Rh, Pd, Au [12–15,17,24–27]. The exact enhancement mechanism is still a subject of discussion, however, two major theories are taken into account. Ligand model theory focuses on the electronic effect of the added metal. According to this model, the alloying metal modifies the electronic structure of platinum valence band and weakens the CO_{ads} binding. Lower energy of metal–CO_{ads} bond allows the adsorbate to be removed more easily [6,28]. In the second theory, the bifunctional mechanism is considered, where platinum atoms are responsible for adsorption of methanol molecules on the catalyst surface, while the second component (e.g., Ru, Rh, Sn) provides active surface oxides, which can oxidize methanol adsorbate at lower potentials [6,28–30], according to the following equations:

$$Pt + CH_3OH \rightarrow Pt\text{–}CO + 4H^+ + 4e^- \quad (5)$$

$$Me + H_2O \rightarrow Me\text{–}OH + H^+ + e^- \quad (6)$$

$$Pt\text{–}CO + Me\text{–}OH \rightarrow Pt + Me + CO_2 + H^+ + e^- \quad (7)$$

Me = Sn, Mo, Ru, Rh, etc.

So far, the best activity in methanol electrooxidation has been shown by Pt–Ru alloys. There are controversies about their optimal composition (Pt:Ru—90:10 vs 50:50), however, all reports confirm a significant decrease in the oxidation potential of the methanol-derived CO_{ads} species (nearly by 200 mV lower than on Pt electrodes) as well as higher current densities obtained during long-term methanol electroxidation at constant potential [24]. In general, the activity of Pt–Ru alloys in methanol oxidation greatly depends on their preparation method (see [6,31–33] for details).

An excellent toleration towards adsorbed CO was found for Pt–Sn alloys by Morimoto and Yeager [34]; nevertheless, Stalnionis et al. [26] have shown that the oxidation of methanol during chronoamperometric experiments on Pt decorated with Sn results in a poor current efficiency. A possible explanation of this phenomenon is that Sn adatoms block active Pt centers required for dehydrogenation of the adsorbate. However, these systems provided interesting data on the oxidation of formic acid and formaldehyde. An increased tolerance towards CO poisoning was also found for the compounds based on Sn, Mo, W, Os and V oxides. Pt–Ru–MeOx or Pt–MeOx interfaces were prepared by fusing the mixture of noble metal halides and transition metal oxides with sodium nitrate at high temperature [35] or by decomposition of polymeric precursors [36]. Pt–Ru–MeOx catalysts showed a significant increase in current density during chronoamperometic experiments but the current related to the mass of catalyst remained low, comparing with a commercial E-TEK Pt–Ru catalyst.

The studies on CO, CO_2 and methanol adsorption and electrooxidation on Pt–Rh electrodes performed by Czerwiński et al. [37,38], Siwek et al. [14] and Tokarz et al. [13] have shown relevant differences in the structure of the corresponding adsorption intermediates. Methanol adsorbate could be removed from the catalyst surface at potentials more positive (by ca. 100 mV) than adsorbed CO and CO_2; however, methanol oxidation potential was by ca. 40 mV lower than on pure Pt electrode.

Pt–Rh–Pd ternary alloys represent an interesting material for an electrocatalyst in Direct Alcohol Fuel Cells (DAFC). Pure palladium has the metal–hydrogen bonding strength similar to that of platinum [39]. Moreover, it has the ability to absorb hydrogen into octahedral vacancy sites [40], thus becomes a potentially promising component responsible for binding and dehydrogenation of alcohol (e.g., methanol) during the electrooxidation process. Furthermore, in contrast to platinum and rhodium, Pd is inactive in CO_2 adsorption above the hydrogen evolution potential. [41]. Earlier studies on Pd-containing alloys (Pt–Pd, Pt–Ru–Pd) also showed a great increase in their activity in formic acid electrooxidation [42]. Current density values obtained during long-term chronoamperometric experiments on Pt–Pd alloys were almost two orders of magnitude higher than obtained on pure Pt electrodes, even though Pt–Pd alloys were less tolerant towards CO poisoning.

In this paper we present the results of the experiments on the electrooxidation of methanol on Pt–Rh–Pd ternary alloys and compare them with the data on the adsorption of CO and CO_2 on these materials. Our goal is to examine the effect of added palladium on the alloy activity in methanol electrooxidation in comparison with Pt and Pt–Rh binary alloys.

2. Experimental

All electrodes used in this study were limited volume electrodes (LVEs) [43–45] prepared by a potentiostatic electrodeposition on a gold wire (99.99% Au; 0.5 mm diameter) from an aqueous bath containing 0.03 M H_2PtCl_6, 0.16 M $RhCl_3$ and 0.01 M $PdCl_2$ in 0.09 M HCl, as reported earlier [46–48]. The composition and thickness of the alloys were controlled by potential and time of electrodeposition. The thickness of the deposited layers was in the range 0.7–2.5 μm and the roughness factor, estimated using the procedure described in Section 3.3 was in the range 50–250. Electrochemical experiments were performed in deoxygenated aqueous 0.5 M H_2SO_4 (electrochemical behavior of Pt–Rh–Pd alloys) or 1 M MetOH in 0.5 M H_2SO_4 (methanol voltammetric stripping and chronoamperometric oxidation) solutions at room temperature. Prior to adsorption or continuous methanol oxidation experiments, the electrodes were cleaned electrochemically by multiple cycling in a wide potential range to obtain well-defined voltammograms. All solutions were prepared from analytical grade reagents and doubly distilled water additionally purified in a Millipore system.

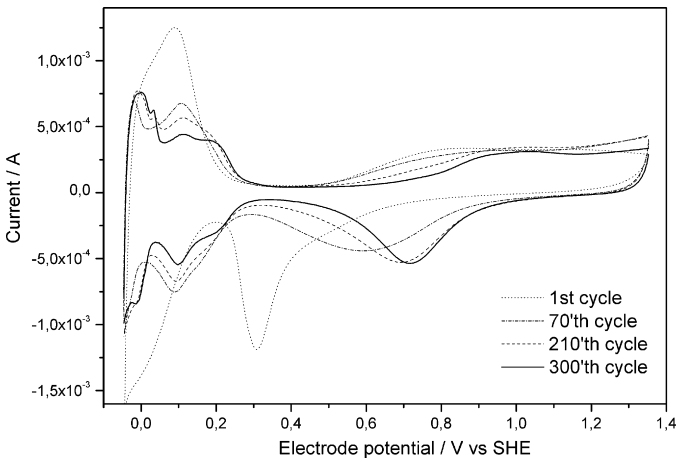

Fig. 1. Cyclic voltammograms (scan rate 0.1 V s^{-1}) recorded in 0.5 M H_2SO_4 for a freshly deposited Pt–Rh–Pd alloy (1st scan) and during electrochemical ageing in a wide potential range (−0.05 to 1.35 V, scan rate 0.1 V s^{-1}). Deposition conditions: potential 0.41 V, time 10 min. Initial alloy bulk composition: 11.0% Pt; 62.4% Rh; 26.6% Pd.

Electrochemical techniques (cyclic voltammetry and chronoamperometry) were performed in a classical three-electrode system with VoltaLab PGZ-301 or CH Instruments 700C potentiostats. Unless noted otherwise, in cyclic voltammetry a scan rate of 0.05 V s^{-1}, an anodic vertex potential of 1.35 V vs the standard hydrogen electrode (SHE) and a cathodic vertex potential of −0.05 V vs SHE were applied. The working electrode potential was measured against mercury/mercury sulfate reference electrode ($Hg|Hg_2SO_4|0.5$ M H_2SO_4) and converted to the SHE scale. A platinum grid was used as the counter electrode.

Bulk compositions of the alloys were analyzed using an EDAX analyzer (EDR-286) coupled with a LEO 435VP scanning electron microscope. Surface compositions were estimated from the potential of surface oxide reduction peak (see Section 3.2 for details). All alloy compositions given in this work are expressed in atomic percentages.

3. Results and discussion

3.1. General electrochemical characteristic of Pt–Rh–Pd alloys

Fig. 1 shows CV responses recorded for a Pt–Rh–Pd electrode (electrodeposited for 600 s at the potential of 0.31 V vs SHE) just after its deposition and during the ageing process, i.e., 350 voltammetric cycles with scan rate of 0.1 V s^{-1} in a wide potential range (from −0.05 to 1.35 V vs SHE). A detailed analysis of the morphology and electrochemical behavior of Pt–Rh–Pd electrodeposits was given in previous works [48]. In general, on the CV curves one can distinguish three characteristic regions, namely: the hydrogen adsorption/absorption/desorption region (the left part of the voltammogram presented in Fig. 1, i.e., at potentials below ca. 0.25 V), the double layer charging region (the mid part of the voltammogram, around ca. 0.40 V) and the oxygen adsorption/desorption (surface oxide formation/reduction) region (the right part of the voltammogram, above ca. 0.30 and 0.50 V in the cathodic and anodic scan, respectively) with a well defined cathodic peak due to surface oxide reduction. This type of CV profiles is characteristic of Pt, Pd, Rh and their alloys, and has been widely described in the literature [49].

The general shape of the CV curves for Pt–Rh–Pd alloys can provide some qualitative data on its surface composition. Fig. 1 demonstrates that the surface of a freshly deposited electrode is covered with a high amount of rhodium, which is mirrored by the presence of a strong, single hydrogen desorption peak and a low potential of the oxygen desorption peak. The shape and position of the latter signal are characteristic of fresh Rh-rich electrodeposits [48,50]. After multiple cyclic polarizations in a wide potential range the initially single hydrogen desorption peak converts into a less intensive, but more complicated signal, consisting of several overlapping peaks [51]. Simultaneously, surface oxides reduction peak shifts into the higher potentials, characteristic of the CV curve for Pt or Pt–Pd alloy surfaces. However, the latter signal remains single, which, according to Woods [49], indicates that the homogeneity of the electrode surface is retained at each stage of the electrochemical ageing process.

As demonstrated earlier [51], a gradual dissolution of less noble metals (Pd and Rh) during alloy surface oxidation results in the change in the surface composition. In the case of Pt–Rh–Pd surfaces this process is also accompanied by the electrode smoothing, which has also been observed previously for various alloy systems [51,52]. Prolonged electrochemical ageing affects the composition of the alloy not only on the surface but also within the subsurface region, which can be detected by EDAX technique. Table 1 summarizes the characteristics of Pt–Rh–Pd alloys used in this study, and the effect of the deposition potential and the ageing process on their bulk compositions, determined by EDAX technique [48].

3.2. In situ estimation of surface composition of Pt–Rh–Pd electrodes

According to the fact that catalytic properties of the alloy electrodes correspond to their surface composition and real surface area, the EDAX data cannot be used as a reliable factor for the electrocatalyst characterization. However, it should be pointed out, that classical surface spectroscopic, high vacuum techniques like Auger electron spectroscopy (AES) or X-ray photoelectron spectroscopy (XPS), albeit useful in materials science research [53], are ex situ methods and therefore they do not allow to monitor the state of the electrode surface under catalyst working conditions (i.e., in a contact with an electrolyte and polarized to a given potential). Thus, for electrocatalytic studies an in situ method of surface characterization is required.

To obtain more reliable information on the surface composition of Pt–Rh–Pd alloys, we have focused on the signal corresponding to surface oxides reduction (oxygen desorption) and adapted the method established earlier by Rand and Woods [49,54] for homogeneous noble metal binary alloys. These authors demonstrated that under the specific conditions of a cyclic voltammetric experiment (type and concentration of the electrolyte, scan rate and potential limits of polarization) the potential of surface oxide reduction peak is different for and thus characteristic of each alloy component [54].

Fig. 2 shows a superposition of CV curves recorded for pure metals (Pt, Rh and Pd) and several Pt–Rh–Pd alloys deposited under different conditions and therefore expected to be characterized by different surface compositions. Indeed, the position of surface oxide reduction peak changes with alloy preparation conditions, being always intermediate with respect to the position of the analogous signals for pure metals. According to Rand and Woods's idea, such a behavior indicates the formation of homogeneous Pt–Rh–Pd alloys of various surface compositions. It should be added that bulk homogeneity of Pt–Rh–Pd electrodeposits was confirmed earlier by XRD measurements and by hydrogen absorption data [55].

As demonstrated in Ref. [48], Rand and Woods's relationship between the surface composition and the potential of surface oxide peak is fulfilled quantitatively also in the case of a Pt–Rh–Pd ternary alloy. Therefore, it is possible to estimate surface contents of the alloy components utilizing the equations for respective binary systems, i.e., Pd–Rh, Pd–Pt or Pt–Rh alloys. A diagram in Fig. 3 shows the atomic fractions of the metals on the alloy surface as a function

Table 1
Experimental conditions during electrodeposition of various Pt–Rh–Pd alloys with their bulk (determined by EDAX technique) and surface compositions (estimated after 30 scans of initial cycling in the range from −0.05 to 1.35 V, 0.1 V s^{-1}), from the potential of surface oxide reduction peak, Eqs. (8)–(10).

	Electrodeposition potential/V vs SHE	Electrodeposition time/s	Bulk composition of fresh electrode [before ageing]/at.%		Bulk composition [after ageing]/at.%		Estimated Rh surface molar fraction limits	Estimated Pt surface molar fraction limits	Estimated Pd surface molar fraction limits
A	0.245	800	Rh Pd Pt	62.4 26.6 11.0	Rh Pd Pt After 540 cycles	15.4 14.1 70.5	0.80–0.84	0.0–0.16	0.0–0.20
B	0.310	600	Rh Pd Pt	46.6 38.0 15.4	Rh Pd Pt After 300 cycles	17.0 21.2 61.8	0.68–0.75	0.0–0.25	0.0–0.32
C	0.410	600	Rh Pd Pt	23.7 45.7 30.6	Rh Pd Pt After 210 cycles	10.9 23.2 65.9	0.0–0.08	0.58–0.92	0.0–0.42
D	0.460	600	Rh Pd Pt	17.2 51.8 31.0	Rh Pd Pt After 700 cycles	4.1 15.4 79.5	0.0–0.03	0.83–0.97	0.0–0.17

of the position of surface oxide reduction peak according to Rand and Woods's relationships for binary systems. Thus, the straight lines represent the limiting surface contents of particular components in a ternary Pt–Rh–Pd alloy characterized by a given value of the potential of surface oxide reduction peak. For instance, in a first approximation, the maximum Rh surface content on Pt–Rh–Pd alloys can be determined from the equation for the Pt–Rh system, while its minimum content can be obtained from the equation for the Pd–Rh system:

$$x_{\mathrm{Rh}}^{\max} = \frac{E_{\mathrm{p}}^{\mathrm{Pt}} - E_{\mathrm{p}}^{\mathrm{alloy}}}{E_{\mathrm{p}}^{\mathrm{Pt}} - E_{\mathrm{p}}^{\mathrm{Rh}}} \tag{8}$$

$$x_{\mathrm{Rh}}^{\min} = \frac{E_{\mathrm{p}}^{\mathrm{Pd}} - E_{\mathrm{p}}^{\mathrm{alloy}}}{E_{\mathrm{p}}^{\mathrm{Pd}} - E_{\mathrm{p}}^{\mathrm{Rh}}} \tag{9}$$

where $E_{\mathrm{p}}^{\mathrm{Pt}}$, $E_{\mathrm{p}}^{\mathrm{Rh}}$, $E_{\mathrm{p}}^{\mathrm{Pd}}$ and $E_{\mathrm{p}}^{\mathrm{alloy}}$ are the potentials of surface oxide reduction peak on pure Pt, Rh, Pd and Pt–Rh–Pd electrodes, respectively. As shown in the diagram, for the whole spectrum of alloy compositions the estimated Rh surface content on Pt–Rh–Pd alloys lies within a rather narrow range between the lines representing Pt–Rh and Pd–Rh binary alloys. In further work we have used the maximum Rh surface atomic fraction obtained from Eq. (8) as a main parameter characterizing the surface composition of the electrodes studied.

The limiting surface contents of Pt or Pd can also be estimated on the basis of the respective relationships for binary systems, however, with a much greater uncertainty, as illustrated in the diagram in Fig. 3. Nevertheless, Pt–Rh–Pd alloys which have been electrodeposited at higher potentials (see Table 1) or have been subjected to ageing process, have a low Rh surface content and therefore they can be treated approximately as Pt–Pd binary alloys. In that case it is possible to estimate the upper limiting Pd surface molar fraction (and lower limiting Pt fraction) according to the equation:

$$x_{\mathrm{Pd}}^{\max} = \frac{E_{\mathrm{p}}^{\mathrm{Pt}} - E_{\mathrm{p}}^{\mathrm{alloy}}}{E_{\mathrm{p}}^{\mathrm{Pt}} - E_{\mathrm{p}}^{\mathrm{Pd}}} \tag{10}$$

where $E_{\mathrm{p}}^{\mathrm{Pd}}$ is the potential of surface oxides reduction peak on pure palladium, and, additionally, to estimate the upper limiting Pt surface molar fraction according to the equation for the

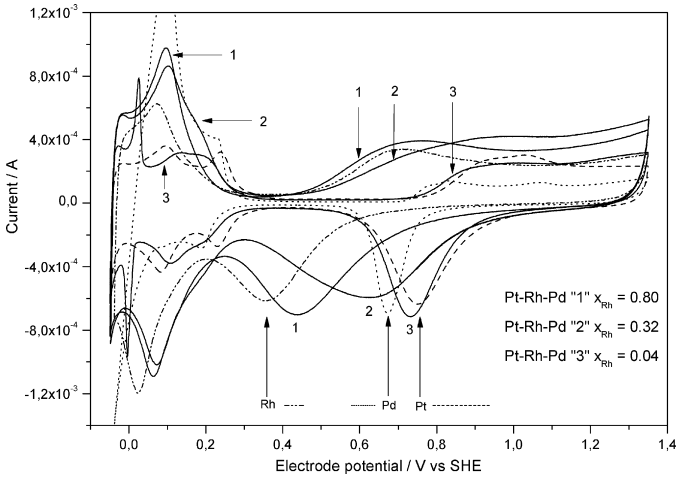

Fig. 2. Cyclic voltammograms (scan rate 0.05 V s^{-1}) recorded in 0.5 M H_2SO_4 for pure components (dashed, dotted and dashed-dotted lines correspond to Pt, Pd and Rh, respectively) and for Pt–Rh–Pd alloys of different initial bulk compositions (solid lines): 1–11.0% Pt; 62.4% Rh; 26.6% Pd; 2–15.4% Pt; 46.6% Rh; 38.0% Pd; 3–30.6% Pt; 23.7% Rh; 45.7% Pd. Rh surface contents, estimated form Eq. (8), indicated in the legend.

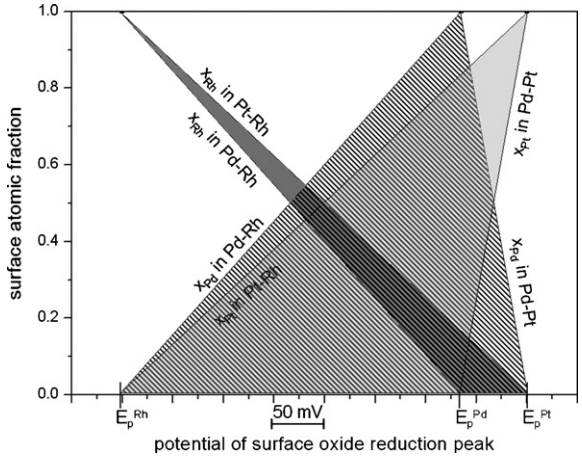

Fig. 3. A diagram showing the relationships between alloy surface composition and the potential of surface oxide reduction peak, according to the idea developed by Rand and Woods [49,54]. The values of peak potentials on pure Rh, Pd and Pt are indicated. Straight lines represent binary systems, filled areas represent a ternary Pt–Rh–Pd system.

Pt–Rh system. Thus, for a given value of the potential of surface oxide reduction peak on a Pt–Rh–Pd ternary alloy one can obtain the ranges of surface content for each alloy component. The most reliable estimations can be made for Rh-rich and Rh-poor electrodes, where the limiting composition ranges are relatively narrow. For alloys with a moderate Rh content the amount of Rh can still be determined with the uncertainty of ca. 10 at.%, while for Pt and Pd only the upper concentrations limits can be known.

The three last columns in Table 1 show the ranges of the values of Rh, Pt and Pd surface molar fractions estimated using Eqs. (8)–(10) from CV curves recorded for the electrodes subjected to 30 potential cycles after their deposition. One can see that the alloy surface compositions can significantly differ from the bulk compositions determined with EDAX technique. For each group of alloys, with the progress of cycling Rh surface content continuously decreased and Pt surface content increased [51]. Thus, as previously concluded, the selective removal of less noble alloy components during potential cycling experiments (mirrored by a positive shift of the oxygen desorption peak) allows to control and modify the surface composition of Pt–Rh–Pd alloys, and thus to obtain materials of a variety of electrocatalytic properties [51].

3.3. Determination of real surface area of Pt–Rh–Pd electrodes

A reliable method of in situ determination of the electrode real surface area (RSA) is crucial for characterization of its catalytic properties and comparison of the catalytic activity of various electrode materials. Classical cyclic voltammetry allows to determine the real surface area of Pt and Rh electrodes by utilizing the charge due to desorption of adsorbed hydrogen:

$$M + H_3O^+ + e^- \rightarrow M\text{–}H_{ads} + H_2O \quad (11)$$

In the case of Pd electrodes due to the simultaneous hydrogen absorption it is difficult to separate the charge originating from hydrogen adsorption only. Instead, the charge due to the formation or reduction of a monolayer adsorbed oxygen (surface oxide) is usually utilized for RSA determination [41].

$$Pd + H_2O \rightarrow Pd\text{–}O_{ads} + 2H^+ + 2e^- \quad (12)$$

In this work we use the fact that each component of the Pt–Rh–Pd alloy has the ability to form well-defined surface oxides. Although in the literature various oxide stoichiometries were earlier postulated for different noble metals, recent results obtained using the EQCM technique [23,50,56] suggest the formation of MO type oxides on Pt, Rh and Pd under the electrochemical conditions in aqueous solutions. According to Rand and Woods [49,54] one can assume that in the case of homogenous Pt–Rh–Pd alloys the electrochemical properties of surface oxides are a linear function of the surface composition. Such a behavior has already been confirmed for the Pd–Au system [57].

The charge due to surface oxide formation or reduction (Q^O) on a Pt–Rh–Pd alloy, measured under fixed experimental conditions (scan rate, anodic potential limit), can be recalculated into the electrode real surface area according to the equation:

$$RSA = \frac{Q^O}{Q^O_{alloy,S} \cdot \theta^O} \quad (13)$$

where $Q^O_{alloy,S}$ is the total charge density corresponding to the formation/reduction of a monolayer of alloy surface oxides on a unitary surface, while θ^O is the alloy surface coverage with the oxide, defined as the ratio between the number of surface atoms covered with oxygen atoms and the total number of surface atoms.

The total charge due to oxidation of a Pt–Rh–Pd surface is the sum of the contributions from the respective components taking into account their relative concentrations on the alloy surface and the values of surface coverage of the individual metals with a MO type oxide:

$$Q^O = 2nF\Sigma(x_M \cdot \theta^O_M) \quad (14)$$

where x_M is the metal (Pt, Rh or Pd) surface molar fraction, θ^O_M is the surface coverage of a given metal with the oxide and n is the number of all active centers on the alloy surface. Since simultaneously the following equation is fulfilled:

$$Q^O = 2nF \cdot \theta^O \quad (15)$$

one can obtain alloy surface coverage with the oxide as a function of the coverages of the individual metals:

$$\theta^O = \Sigma(x_M \cdot \theta^O_M) \quad (16)$$

The full expression for the denominator in Eq. (13) can be obtained taking into account that the charge densities due to the formation/reduction of a monolayer of the surface oxides on pure Pt, Rh and Pd electrodes are in the range of 420–442 μC cm^{-2}, which leads to the following assumption:

$$Q^O_{Pt,S} \approx Q^O_{Pd,S} \approx Q^O_{Rh,S} \approx Q^O_{ML,S} = Q^O_{alloy,S} \quad (17)$$

and therefore:

$$RSA = \frac{Q^O}{\Sigma(Q^O_{ML,S} \cdot x_M \cdot \theta^O_M)} \quad (18)$$

The estimation of the real surface area using Eq. (18) requires the pre-determination of the values of surface coverage with the oxide for pure alloy components under the same experiments conditions (anodic vertex potential and scan rate in a cyclic voltammetric experiment, electrolyte composition and concentration) as in the case of the alloys. The estimated values of the oxygen surface coverage obtained during independent experiments (data not shown) were 0.62, 0.95 and 0.80 for pure platinum, rhodium and palladium electrodes, respectively (at the same anodic vertex potential of 1.35 V).

3.4. Methanol adsorption and stripping on Pt–Rh–Pd electrodes

Fig. 4 presents cycling voltammograms recorded after methanol adsorption at 0.26 V vs SHE for 30 min on Pt–Rh–Pd alloys rich and poor in Rh on the surface (Fig. 4A and B, respectively). As in the case of CO_2 and CO adsorption, in the presence of adsorbed methanol there is a significant decrease in currents in the hydrogen electrosorption region. However, it should be noted that the signals due to the oxidation of mainly absorbed hydrogen (in the range from −0.05 to 0.05 V vs SHE) are essentially undisturbed by the methanol adsorbate. The same effect was observed for CO_2 adsorption on Pt–Rh–Pd alloys [58]. This behavior suggests that the presence of adsorbed methanol on Pt–Rh–Pd alloys affects hydrogen adsorption only. This fact enables to determine the parameter of electron per site from cyclic voltammograms (see text below).

It is worth noting that in the case of Pt–Rh–Pd alloys enriched with rhodium on the surface the onset of the methanol oxidation overlaps with the initial stages of surface oxide formation. On the other hand, rhodium-depleted Pt–Rh–Pd alloys are able to start oxidizing methanol at the potentials from the double layer region, i.e., before the oxide formation begins. Nevertheless, in both cases methanol oxidation signals are single and well defined, however, with different peak amplitudes and widths, dependent on alloy surface composition.

The position of the peak due to the oxidation of adsorbed methanol also depends on alloy surface composition. Fig. 5 shows the relationship between the peak potential and Rh surface molar

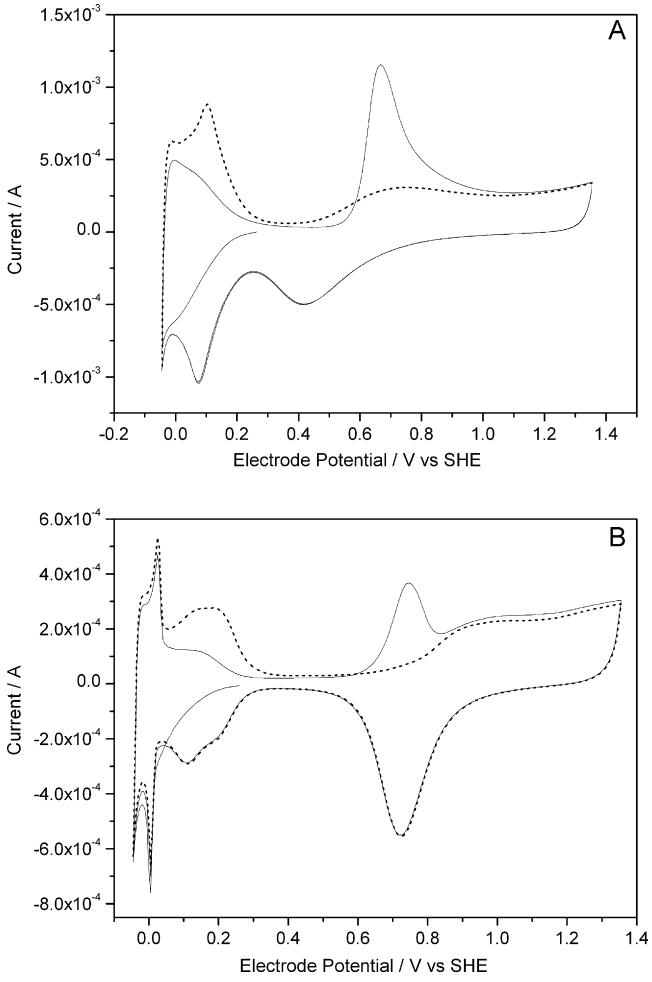

Fig. 4. Cyclic voltammograms (scan rate 0.05 V s^{-1}) recorded in 0.5 M H_2SO_4 after 30 min of methanol adsorption at 0.26 V on Rh Pt–Rh–Pd alloys of different surface Rh contents: (a) Rh-rich alloy, x_{Rh} = 0.85, (b) Rh-poor, x_{Rh} = 0.07. Solid line—first cycle after adsorption and dotted line—second cycle after adsorption (background).

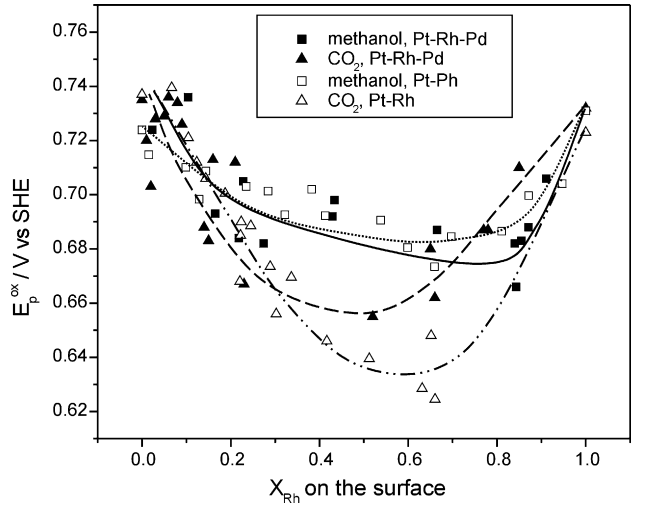

Fig. 5. Stripping peak potential, E_p^{ox} vs Rh surface content, x_{Rh} calculated from Eq. (8) for methanol and CO_2 adsorption (in separate experiments) on Pt–Rh (data from [13,14]) and Pt–Rh–Pd electrodes. Scan rate: 0.05 V s^{-1}, adsorption potential and time: 0.02 V/45 min for CO_2, and 0.26 V/30 min for methanol.

fraction, for methanol electrooxidation on Pt–Rh–Pd alloys compared with the data for methanol on Pt–Rh alloys and adsorbed CO_2 on both Pt–Rh–Pd and Pt–Rh alloys [13,14]. The general trend for methanol adsorbed on Pt–Rh–Pd ternary alloys is similar to that found earlier on Pt–Rh binary alloys [13,14]. As demonstrated in Fig. 5, the potential of adsorbed methanol oxidation peak on Pt–Rh–Pd alloys decreases with increasing Rh surface content from ca. 0.74 V vs SHE for Rh-poor alloys to a minimum value of ca. 0.67 V for alloys containing ca. 80–85% Rh on the surface, followed by a rapid increase in the peak potential for Rh-rich alloys. The negative shift in methanol oxidation potential on Pt–Rh–Pd alloys is slightly greater (by ca. 20 mV) than for Pt–Rh alloys [13,14] and the minimum value of the peak potential also corresponds to a different surface Rh content as compared to Pt–Rh alloys.

The above behavior may be qualitatively explained assuming that due to the existence of additional amounts of Pd surface atoms the electronic structure of the Pt–Rh–Pd alloy is slightly modified with respect the Pt–Rh alloy, which allows the bond between the metal and adsorbed methanol to be weakened. It is noteworthy that the effect of Pd addition on methanol adsorption is in the opposition to the tendency of the changes in the alloy activity in the oxidation of the product of CO_2 adsorption (see Fig. 5). In the latter case even a small addition of Pd to the Pt–Rh binary system made the oxidation of the carbonaceous adsorbate on Pt–Rh–Pd alloys more difficult than on Pt–Rh alloys, although for certain alloy compositions this process still occurred more easily than on pure Pt or Rh (see [15] for details). It is thus possible that Pd has an additional effect on the adsorbate structure, which affects the kinetics of its oxidation.

A deeper insight into the process of methanol adsorption and electrooxidation on Pt–Rh–Pd alloys of various compositions requires a closer look at the adsorbates structure via the analysis of the values of electron per site (*eps*) parameter. In general, *eps* value corresponds to the number of electrons exchanged between the electrode and the adsorbate during its oxidation process related to one surface active center occupied by the adsorbate. Due to the aforementioned fact that adsorbed methanol does not affect the process of hydrogen absorption into Pt–Rh–Pd alloys, under the conditions of a cyclic voltammetric experiment the *eps* parameter can be calculated according to the equation:

$$eps = \frac{Q_{MetOH}^{Ox}}{Q_{H,max} - Q_{H,min}} \quad (19)$$

where Q_{MetOH}^{Ox} is the charge corresponding to the oxidative removal of adsorbed methanol, $Q_{H,max}$ is the charge of hydrogen desorption in the absence of adsorbed methanol and $Q_{H,min}$ is the charge of hydrogen desorption in the presence of adsorbed methanol.

Fig. 6 shows the influence of Rh concentration on the surface of Pt–Rh–Pd alloys on the values of *eps* obtained for the oxidation of the product of methanol adsorption, in comparison with data for the products of CO_2 and CO adsorption. In the case of methanol adsorption *eps* values increase from ca. 1.1 to 2.3 with increasing Rh surface content, particularly rapidly for electrodes poor in Rh and slightly for the electrodes rich in Rh. A qualitatively similar course of the dependence of *eps* on alloy surface composition is observed in the case of the product of CO_2 adsorption, where *eps* values range from 1.2 to 2.3. However, for almost all alloy compositions the values of *eps* for adsorbed CO_2 are higher than those for the product of methanol adsorption. On the other hand, a different relationship between *eps* and Rh surface content is visible in the case of adsorbed CO. For this adsorbate a rather parabollic curve is observed with *eps* values ranging from 1.5 to 2, and a flat minimum at moderate Rh surface content (ca. 50%). Moreover, for the electrodes poor in Rh on the surface *eps* values for adsorbed CO are higher than those for adsorbed methanol and CO_2, while for other alloy compositions these values are lower.

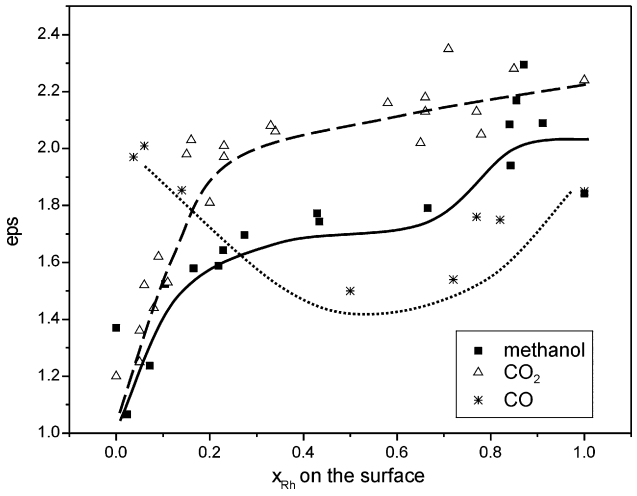

Fig. 6. Electron per site *eps* vs Rh surface content, x_{Rh} calculated from Eq. (8) for methanol, CO and CO_2 adsorption (in separate experiments) on Pt–Rh–Pd electrodes. Scan rate: 0.05 V s^{-1}, adsorption potential and time: 0.02 V/20 min for CO, 0.02 V/45 min for CO_2, and 0.26 V/30 min for methanol.

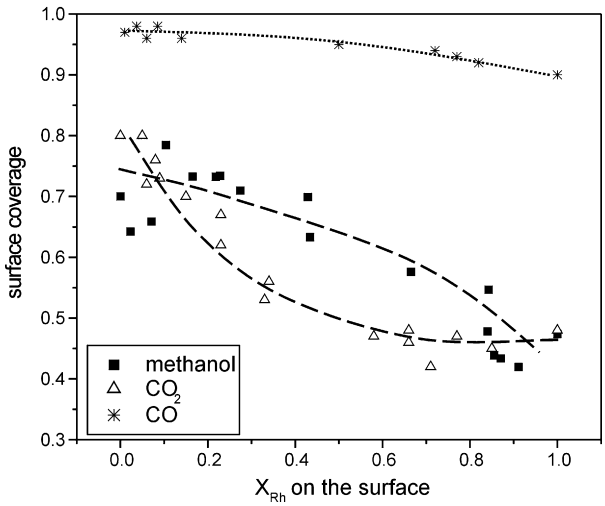

Fig. 7. Surface coverage θ vs Rh surface content, x_{Rh} calculated from Eq. (8) for methanol, CO and CO_2 adsorption (in separate experiments) on Pt–Rh–Pd electrodes. Scan rate: 0.05 V s^{-1}, adsorption potential and time: 0.02 V/20 min for CO, 0.02 V/45 min for CO_2, and 0.26 V/30 min for methanol.

The values of *eps* contain the information on the structure of the adsorbate. Assuming after the literature that the main products of methanol adsorption are CO species, the changes in *eps* from ca. 1.1 to 2 with increasing Rh surface content can be ascribed to the increase in the relative contribution of linearly bonded CO molecules (═CO, *eps* = 2) at the expense of bridge bonded ones (>CO, *eps* = 1). However, *eps* values higher than 2 obtained for Rh-rich electrodes indicate the existence of some amounts of additional species more reduced than CO, possibly CHO or ≡COH radicals (*eps* = 3). This explanation has been proposed for the tendency observed for adsorbed CO_2 [15], although in that case at a given electrode composition the contribution of ═CO and/or ≡COH/CHO species seems to be greater than for the methanollic adsorbate. Nevertheless, the similar courses of *eps* vs alloy composition dependence for CO_2 and methanol suggest higher similarity between both these adsorbates than with the product of a direct CO adsorption. In the latter case probably the proportions between linearly and bridge bonded CO are much more different and the composition of minor products might also differ from that for adsorbed methanol and CO_2. Our results for Pt–Rh–Pd alloys are in line with other authors' findings [59–63] for Pt electrode that adsorbed CO_2 is more similar (although not identical) to the products of methanol, formaldehyde and formic acid adsorption than to directly adsorbed CO. The differences between adsorbed CO_2 and CO on platinum group metals and alloys have been discussed in detail in our earlier papers [13–15,37,38,64–70].

A second source of the information on the adsorbate properties is the value of surface coverage with the adsorbate on Pt–Rh–Pd electrodes of different surface compositions. In general, surface coverage is given by the following equation:

$$\theta = \frac{n_M^{occ}}{n} \tag{20}$$

where n_M^{occ} is the number of catalytic sites occupied by the adsorbate. As in the case of *eps* parameter, θ value can be estimated on the basis of hydrogen oxidation charges in the presence and absence of adsorbed methanol:

$$\theta = \frac{Q_{H,max} - Q_{H,min}}{Q_{H,max}^{ads}} \tag{21}$$

where $Q_{H,max}^{ads}$ is the maximum charge due to the oxidation of adsorbed hydrogen only. For pure Pt and Rh the latter charge is equal to $Q_{H,max}$ since only hydrogen adsorption is possible. The situation is different for materials with the ability to absorb hydrogen (as for Pd and its alloys). In that case anodic signals placed in the hydrogen potential range originate from both adsorbed and absorbed hydrogen oxidation, which makes it more difficult to estimate θ from cylic voltammograms. However, according to earlier results the anodic hydrogen peak placed at the lowest potential range (between −0.05 and 0.05 V) can be attributed mainly to the removal of absorbed hydrogen, while signals at higher potentials (above ca. 0.05 V) are mainly due to desorption of adsorbed hydrogen [15]. As it was showed above, methanol adsorbate does not significantly block hydrogen absorption into Pt–Rh–Pd alloys, thus the difference in the numerator in Eq. (21) can be ascribed to the changes in the charge due to hydrogen adsorption. The contribution from adsorbed hydrogen oxidation ($Q_{H,max}^{ads}$) was estimated by deconvolution of multiple current peaks using Microcal Origin® software. The correctness of this method was confirmed by independent calculations of $Q_{H,max}^{ads}$ from a half of the charge corresponding to the formation of a monolayer of surface oxide.

Fig. 7 presents the values of surface coverage with adsorbed methanol as a function of Rh surface content in comparison with the analogous data obtained in separate experiments with CO_2 and CO adsorption on Pt–Rh–Pd alloys. The values of surface coverage with adsorbed CO_2 and methanol are of the same order, in both cases decreasing from ca. 0.80 for low Rh content to 0.45 for the highest x_{Rh}. However, the curve obtained for CO_2 adsorption drops more rapidly with increasing Rh surface content and then reaches a plateau at $x_{Rh} = 0.6$, while for methanol the changes in θ are more linear. On the other hand, surface coverage with adsorbed CO is much higher (above 0.90) and only weakly dependent on alloy composition. These variations could be explained by different adsorbate structures and mechanisms of CO_2, CO and CH_3OH adsorption. As it was reported in the literature, adsorption of CO_2 requires the presence of adsorbed hydrogen as a reductive factor. However, it should be added that this condition is necessary both not sufficient, as CO_2 can be reduced by underpotentially deposited (UPD) hydrogen (i.e., at potentials positive to hydrogen evolution potential) only on Pt, Rh and their alloys (see [70]). On the contrary, directly adsorbed CO tends to occupy nearly all available adsorption sites, i.e., both Pt or Rh and Pd surface atoms, and the presence of adsorbed hydrogen is not necessary for this process to occur. In turn, adsorption of methanol requires breaking the C–H bonds in the first step which primarily distinguishes it from the gaseous CO and CO_2 adsorption

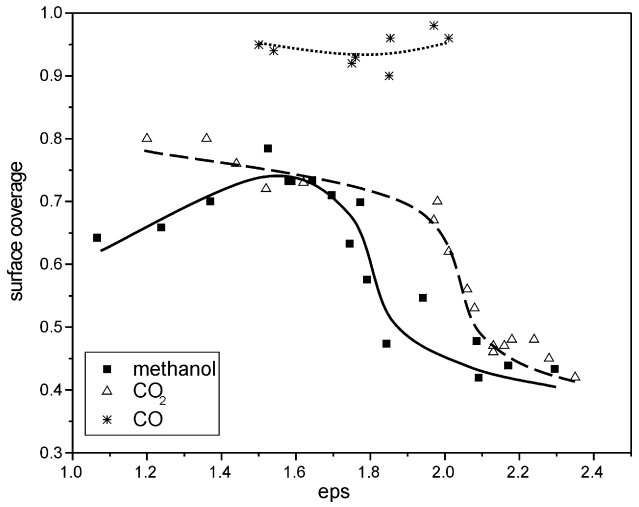

Fig. 8. Surface coverage θ vs electron per site *eps* for methanol, CO and CO_2 adsorption (in separate experiments) on Pt–Rh–Pd electrodes. Scan rate: 0.05 V s^{-1}, adsorption potential and time: 0.02 V/20 min for CO, 0.02 V/45 min for CO_2, and 0.26 V/30 min for methanol.

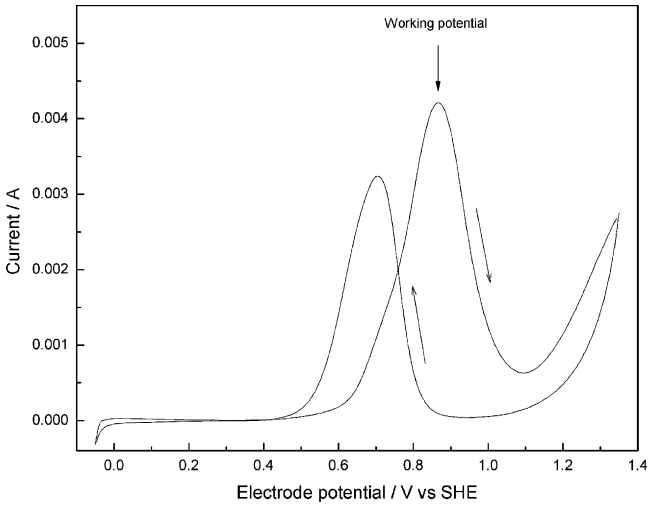

Fig. 9. Schematic diagram illustrating the cyclic voltammogram of studied electrodes in 1 M CH_3OH/0.5 M H_2SO_4 obtained prior to main chronoamperometric experiments. Potentials of CA measurements were set separately for each Pt–Rh–Pd electrode (working potential—potential of the maximum methanol oxidation current obtained during positive voltammetric scan, $\nu = 0.05$ V s^{-1}).

process. Additionally, the presence of H-UPD on the electrode surface inhibits the formation of methanol adsorbate, indicating lower surface coverage in the case of adsorption in hydrogen UPD region [13,14].

Fig. 8 demonstrates the interrelation between *eps* and θ values for the adsorbates considered above. One should note that in the case of adsorbed CO_2 and methanol the trends are again more similar to each other than to the tendency observed for adsorbed CO. Lower surface coverage with these adsorbates is related to higher *eps*, i.e., the domination of linearly bonded CO, characteristic of Rh-rich electrodes, while higher θ values are accompanied by lower *eps*, i.e., a greater contribution from bridge bonded CO. Probably the decrease in surface coverage with *eps* results from steric effects, which become more important when linearly bonded CO dominate on the surface together with some amounts of such more bulky structures like COH or CHO radicals. The possibility of these additional species among CO-type adsorbate is in line with a rapid drop of surface coverage for higher *eps*, suggesting a qualitative change in the adsorbate structure (see also [65] for details).

3.5. Continuous oxidation of methanol on Pt–Rh–Pd electrodes

In order to compare catalytic properties of Pt–Rh–Pd alloys in direct methanol oxidation the long-term chronoamperometric experiments were performed. Prior to main experiments, few cyclic voltammetry ($\nu = 0.05$ V s^{-1}) scans in 0.5 M H_2SO_4 containing 1 M CH_3OH were obtained in order to determine the working potential at which methanol oxidation current densities were the highest for the studied Pt–Rh–Pd electrodes (see Fig. 9).

Fig. 10 presents the results of continuous methanol oxidation on pure Pt electrode and Pt–Rh–Pd alloys of various compositions, as listed in Table 1. In the case of electrodes highly enriched with rhodium (Pt–Rh–Pd "A"), methanol oxidation current densities were almost two orders of magnitude lower as compared to pure Pt. In addition, a rapid current drop suggests worse resistance to CO poisoning, which is in agreement with the low activity of pure Rh electrodes. The activity enhancement is noticeable for the electrodes with a significant increase in the surface amount of platinum and palladium (Pt–Rh–Pd "B, C and D" alloys). However, without the precise knowledge on the exact Pt/Pd surface ratio it is difficult to determine the structure of catalytic sites responsible for effective methanol adsorption. The comparison of currents densities for "B",

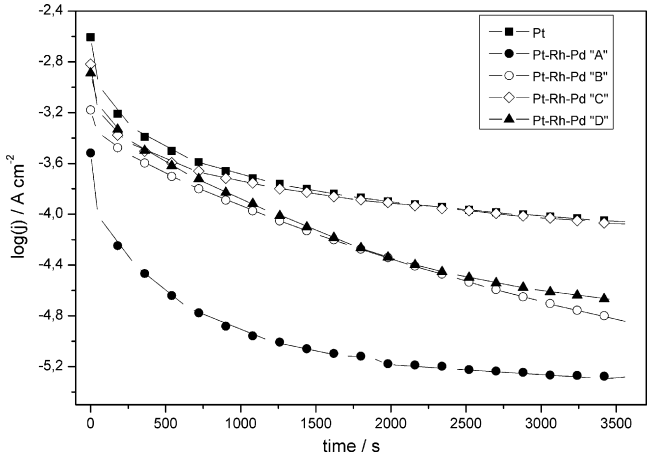

Fig. 10. Chronoamperometric curves obtained during 60 min of continuous oxidation of methanol (1 M CH_3OH/0.5 M H_2SO_4) on Pt–Rh–Pd electrodes of different bulk compositions and Rh surface contents: A—11.0% Pt; 62.4% Rh; 26.6% Pd (x_{Rh} = 0.85, working potential = 0.722 V); B—15.4% Pt; 46.6% Rh; 38.0% Pd (x_{Rh} = 0.65, working potential = 0.785 V); C—30.6% Pt; 23.7% Rh; 45.7% Pd (x_{Rh} = 0.08, working potential = 0.920 V); D—31.0% Pt; 17.2% Rh; 51.8% Pd (x_{Rh} = 0.03, working potential = 0.879 V); pure Pt electrode working potential = 0.866 V.

"C" and and "D" alloys suggests that a moderate addition of Pd into Pt–Rh alloys with a moderate Rh or high Pt contents could modify the alloy electronic structure enough to weaken metal–CO bonding strength. However, the effective activity of continuous methanol oxidation still does not exceed its counterpart for pure Pt.

Considering the data obtained during stripping experiments one could expect a much better activity in continuous methanol oxidation for Rh-rich Pt–Rh–Pd alloys, which is in opposition to the results shown in Fig. 10. An explanation for an analogical situation for Pt–Rh binary alloys was proposed by Tokarz et al. [13]. According to those authors, one should take into account that the oxidation of adsorbed methanol after 30 min of adsorption time delivers data on the electrochemical properties (mirrored in the oxidation potential and charge) of the final adsorption product, i.e., determining its thermodynamic stability but giving no information about adsorption/oxidation kinetics. In the case of Rh-rich Pt–Rh–Pd electrodes (x_{Rh} = 0.84), dehydrogenation of methanol is considered as the rate determining step (see Eq. (1)) due to their coverage vs adsorp-

tion time behavior, which was similar to pure Rh electrodes (data not shown). The adsorbate saturation was obtained after 40 min of adsorption time (final value $\theta = 0.54$) while for the other compositions (namely "B", "C" and "D" alloys) its value remained constant even for very short adsorption time (e.g., 5 min). This fact suggests that the increase in platinum and palladium surface content contributes in changing the rate determining step to the formation of active surface oxides (see Eq. (2)) and/or recombination process (Eq. (3)). Although "B" and "D" alloys show significant differences between Rh surface content ($x^{B}_{Rh} = 0.65$, $x^{D}_{Rh} = 0.03$), in both cases current densities of continuous methanol oxidation are of the same order. Second difference between them is the value of their "working potential". In the case of Pt–Rh–Pd "B" alloy, maximum current density of methanol continuous oxidation was obtained at 0.785 V, while for the alloy significantly impoverished in Rh ("D") working potential was of the value 0.879 V—almost the same as for pure Pt electrode (0.866 V). Since the bottleneck of methanol oxidation on platinum is the adsorption of OH species [6] it is likely that lowering of methanol oxidation potential on Pt–Rh–Pd "B" alloy could be related to the formation of rhodium surface oxides (RhO) at lower potentials which is required to remove methanol adsorbate via bifunctional mechanism (in this case adsorption of methanol should occur at Pt or Pt–Pd rather than Rh sites). On the other hand, Pt–Rh–Pd "C" alloy shows almost identical current densities as pure Pt electrode, however the continuous oxidation potential was set at 0.920 V which was significantly higher, thus it is very difficult to determine the exact rate determining step on the basis of the information given above. Nevertheless, our results suggest the existence of an optimal composition of Pt–Rh–Pd alloys where both the electronic effect (Pt–Pd interaction) and the bifunctional mechanism contribute to a high activity in methanol oxidation. It is noteworthy that a similar phenomenon was observed for Sn decorated Pt and Pt–Sn high surface area alloys. In the former case surface Sn adatoms significantly blocked Pt active centers inhibiting methanol dehydrogenation step which contributed in a rapid decrease in continuous methanol oxidation currents [26]. This state may correspond to our Pt–Rh–Pd electrodes with the highest Rh surface molar fraction (Pt–Rh–Pd "A" alloys). On the other hand, high surface area Pt–Sn alloys (Pt:Sn = 3:1) showed enhanced activity in methanol oxidation, compared to most active Pt–Ru catalyst [34] indicating that Sn surface active oxides facilitate electrodesorption of the methanol adsorbate via bifunctional mechanism.

4. Conclusions

Pt–Rh–Pd ternary alloys demonstrated different catalytic activities in methanol adsorption and oxidation depending on their surface compositions. Methanol adsorption did not affect the absorption of hydrogen into Pt–Rh–Pd electrodes which was found to be useful in estimation of values of the electron per site and surface coverage with the adsorbate. Methanol adsorption process led to creation of a mixture of mainly linearly and bridge bonded CO, however, being more similar to the product of CO_2 adsorption rather than directly adsorbed CO. The best activity in oxidation of adsorbed methanol during stripping experiments was found for Pt–Rh–Pd alloys with maximal 80% surface rhodium content, where the adsorbate oxidation peak shifted negatively by 60 mV as compared to pure Pt electrode. Continuous methanol oxidation revealed strong inhibition of methanol adsorption and oxidation process in the case of most Pt–Rh–Pd compositions. The rate determining step was changing from the dehydrogenation of methanol to formation of oxygen species and recombination process with the lower surface Rh content, suggesting mixed contribution of electronic effect and bifunctional mechanism into the methanol oxidation process.

Acknowledgement

Statutory funding from the Industrial Chemistry Research Institute in Warsaw is greatly acknowledged.

References

[1] W.R. Grove, Phil. Mag. J. Sci. XIV (1839) 127–130.
[2] P. Zelenay, P. Piela, Fuel Cell Rev. 1 (2004) 17–23.
[3] A.S. Aricò, S. Srinivasan, V. Antonucci, Fuel Cells 1 (2001) 133–161.
[4] C. Lamy, E.M. Belgsir, J.-M. Léger, J. Appl. Electrochem. 31 (2001) 799–809.
[5] T.R. Ralph, M.P. Hogarth, Platinum Metals Rev. 46 (2002) 3–14.
[6] A. Hamnett, Catal. Today 38 (1997) 445–457.
[7] T. Iwasita, in: W. Vielstich, H.A. Gasteiger, A. Lamm (Eds.), Handbook of Fuel Cells—Fundamentals, Technology and Applications, John Wiley & Sons, 2003, pp. 603–624.
[8] F. Vidal, B. Busson, C. Six, O. Pluchery, A. Tadjeddine, Surf. Sci. 502–503 (2002) 485–489.
[9] J.-M. Léger, J. Appl. Electrochem. 31 (2001) 767–771.
[10] F. Seland, T. Reidar, D.A. Harrington, Electrochim. Acta 51 (2006) 3827–3840.
[11] J.T. Müller, P.M. Urban, W.F. Hölderich, J. Power Sources 84 (1999) 157–160.
[12] W. Tokarz, P. Piela, A. Czerwiński, J. Solid State Electrochem. 14 (2010) 515–521.
[13] W. Tokarz, P. Piela, A. Czerwiński, Electrochim. Acta 52 (2007) 5565–5573.
[14] H. Siwek, W. Tokarz, P. Piela, A. Czerwiński, J. Power Sources 181 (2008) 24–30.
[15] M. Łukaszewski, A. Czerwiński, J. Electroanal. Chem. 606 (2007) 117–133.
[16] Z. Jusys, J. Kaiser, R.J. Behm, Electrochim. Acta 47 (2002) 3693–3706.
[17] H. Massong, H. Wang, G. Samjeske, H. Baltruschat, Electrochim. Acta 46 (2001) 701–707.
[18] D. Kardash, C. Korzeniewski, N. Markovic, J. Electroanal. Chem. 500 (2001) 518–523.
[19] H.Y.H. Chan, C.T. Williams, M.J. Weaver, C.G. Takoudisz, J. Catal. 174 (1998) 191–200.
[20] J.G. Love, P.A. Brooksby, A.J. McQuillan, J. Electroanal. Chem. 464 (1999) 93–100.
[21] A. Miki, S. Ye, T. Senzaki, M. Osawa, J. Electroanal. Chem. 563 (2004) 23–31.
[22] P. Waszczuk, A. Wieckowski, P. Zelenay, S. Gottesfeld, C. Coutanceau, J.-M. Léger, C. Lamy, J. Electroanal. Chem. 511 (2001) 55–64.
[23] G. Jerkiewicz, G. Vatankhah, J. Lessard, M.P. Soriaga, Y.-S. Park, Electrochim. Acta 49 (2004) 1451–1459.
[24] P. Waszczuk, J. Solla-Gull, H.-S. Kim, Y.Y. Tong, V. Montiel, A. Aldaz, A. Wieckowski, J. Catal. 203 (2001) 1–6.
[25] O. Yépez, G. Pickup, Electrochem. Solid-State Lett. 8 (2005) 35–38.
[26] G. Stalnionis, L. Tamašauskaité-Tamašiūnaitė, V. Pautienienė, Z. Jusys, Solid State Electrochem. 8 (2004) 900–907.
[27] Z. Borkowska, A. Tymosiak-Zielinska, G. Shul, Electrochim. Acta 49 (2004) 1209–1220.
[28] M. Watanabe, S. Motoo, J. Electroanal. Chem. 60 (1975) 275–283.
[29] S.Lj. Gojković, T.R. Vidaković, D.R. Durović, Electrochim. Acta 48 (2003) 3607–3614.
[30] P. Waszczuk, G.-Q. Lu, A. Wieckowski, C. Lu, C. Rise, R.I. Masel, Electrochim. Acta 47 (2002) 3637–3652.
[31] A.N. Gavrilov, O.A. Petrii, A.A. Mukovnin, N.V. Smirnova, T.V. Levchenko, G.A. Tsirlina, Electrochim. Acta 52 (2007) 2775–2784.
[32] Y. Zhao, Y. Cai, J. Tian, H. Lan, Mater. Chem. Phys. 115 (2009) 831–834.
[33] A.L. Zhu, M.Y. Teo, S.A. Kulinich, Appl. Catal. A 352 (2009) 17–26.
[34] Y. Morimoto, E.B. Yeager, J. Electroanal. Chem. 444 (1998) 95–100.
[35] Z. Jusys, T.J. Schmidt, L. Dubau, K. Lasch, L. Jörissen, J. Garche, R.J. Behm, J. Power Sources 105 (2002) 297–304.
[36] M.B. de Oliveira, L.P.R. Profeti, P. Olivi, Electrochem. Commun. 7 (2005) 703–709.
[37] A. Czerwiński, J. Sobkowski, A. Karczmarek, M. Nowakowska, Anal. Lett. 18 (1985) 1465–1477.
[38] A. Czerwieński, J. Sobkowski, Anal. Lett. 17 (1984) 2175–2181.
[39] J.O'.M. Bockris, A.K.N. Reddy, M. Gamboa-Aldeco, Modern Electrochemistry, vol. 2A, 2nd ed., Kluwer/Plenum, New York, 2000, p. 1285.
[40] G. Jerkiewicz, A. Zolfaghari, J. Electrochem. Soc. 143 (1996) 1240–1248.
[41] A. Czerwiński, J. Electroanal. Chem. 379 (1994) 487–493.
[42] P. Waszczuk, T.M. Barnard, C. Rice, R.I. Masel, A. Wieckowski, Electrochem. Commun. 4 (2002) 599–603.
[43] A. Czerwiński, R. Marassi, S. Zamponi, J. Electroanal. Chem. 316 (1991) 211–221.
[44] A. Czerwiński, R. Marassi, J. Electroanal. Chem. 322 (1992) 373–381.
[45] A. Czerwiński, Electrochim. Acta 39 (1994) 431–436.
[46] M. Grdeń, A. Paruszewska, A. Czerwiński, J. Electroanal. Chem. 502 (2001) 91–99.
[47] M. Łukaszewski, M. Grdeń, A. Czerwiński, J. Phys. Chem. Solids 65 (2004) 523.
[48] M. Łukaszewski, A. Czerwiński, Thin Solid Films 518 (2010) 3680–3689.
[49] R. Woods, in: A.J. Bard (Ed.), Electroanal. Chem., vol. 9, Marcel Dekker, New York, 1976.
[50] M. Łukaszewski, H. Siwek, A. Czerwiński, Electrochim. Acta 52 (2007) 4560–4565.
[51] M. Łukaszewski, M. Grdeń, A. Czerwiński, J. Solid State Electrochem. 9 (2005) 1–9.
[52] M. Łukaszewski, A. Czerwiński, Electrochim. Acta 48 (2003) 2435–2445.
[53] M. Pisarek, M. Łukaszewski, M. Janik-Czachor, Pol. J. Chem. 83 (2009) 1393–1412.

[54] D.A.J. Rand, R. Woods, J. Electroanal. Chem. 36 (1972) 57–69.
[55] M. Łukaszewski, M. Grdeń, A. Czerwiński, J. Electroanal. Chem. 573 (2004) 87–98.
[56] M. Tian, B.E. Conway, J. Electroanal. Chem. 581 (2005) 176–189.
[57] M. Łukaszewski, A. Czerwiński, J. Solid State Electrochem. 12 (2008) 1589–1598.
[58] M. Łukaszewski, M. Grdeń, A. Czerwiński, Electrochim. Acta 49 (2004) 3161–3167.
[59] V.N. Kamath, H. Lal, J. Electroanal. Chem. 19 (1968) 137–145.
[60] J. Willsau, J. Heitbaum, Electrochim. Acta 31 (1986) 943–948.
[61] Yu.B. Vassiliev, V.S. Bagotzky, N.V. Osetrova, A.A. Mikhailova, J. Electroanal. Chem. 189 (1985) 311–324.
[62] V.E. Kazarinov, V.N. Andreev, A.V. Shlepakov, Electrochim. Acta 34 (1989) 905–913.
[63] D.C. Papageorgopoulos, F.A. de Bruijn, J. Electrochem. Soc. 149 (2002) A140–A145.
[64] M. Łukaszewski, A. Czerwiński, J. Solid State Electrochem. 11 (2007) 339–349.
[65] H. Siwek, M. Łukaszewski, A. Czerwiński, Phys. Chem. Chem. Phys. 10 (2008) 3752–3765.
[66] M. Łukaszewski, A. Czerwiński, Electrochim. Acta 51 (2006) 4728–4735.
[67] A. Czerwiński, J. Sobkowski, J. Electroanal. Chem. 91 (1978) 47–53.
[68] J. Sobkowski, A. Więckowski, P. Zelenay, A. Czerwiński, J. Electroanal. Chem. 100 (1979) 781–790.
[69] J. Sobkowski, A. Czerwiński, J. Phys. Chem. 89 (1985) 365–369.
[70] M. Łukaszewski, H. Siwek, A. Czerwiński, J. Solid State Electrochem. 13 (2009) 813–827.